Orbitally induced oscillations in the East Antarctic ice sheet at the Oligocene/Miocene boundary

Tim R. Naish[1], Ken J. Woolfe[2,3], Peter J. Barrett[4], Gary S. Wilson[5], Cliff Atkins[4], Steven M. Bohaty[6], Christian J. Bücker[7,8], Michele Claps[9,8], Fred J. Davey[1], Gavin B. Dunbar[2,4], Alistair G. Dunn[10], Chris R. Fielding[11], Fabio Florindo[12,13], Michael J. Hannah[4], David M. Harwood[6], Stuart A. Henrys[1], Lawrence A. Krissek[14], Mark Lavelle[15], Jaap van der Meer[16,8], William C. McIntosh[17], Frank Niessen[18], Sandra Passchier[14], Ross D. Powell[19], Andrew P. Roberts[13], Leonardo Sagnotti[12], Reed P. Scherer[19], C. Percy Strong[1], Franco Talarico[20], Kenneth L. Verosub[21], Giuliana Villa[22], David K. Watkins[6], Peter-N. Webb[14] & Thomas Wonik[7]

Between 34 and 15 million years (Myr) ago, when planetary temperatures were 3–4 °C warmer than at present and atmospheric CO_2 concentrations were twice as high as today[1], the Antarctic ice sheets may have been unstable[2–7]. Oxygen isotope records from deep-sea sediment cores suggest that during this time fluctuations in global temperatures and high-latitude continental ice volumes were influenced by orbital cycles[8–10]. But it has hitherto not been possible to calibrate the inferred changes in ice volume with direct evidence for oscillations of the Antarctic ice sheets[11]. Here we present sediment data from shallow marine cores in the western Ross Sea that exhibit well dated cyclic variations, and which link the extent of the East Antarctic ice sheet directly to orbital cycles during the Oligocene/Miocene transition (24.1–23.7 Myr ago). Three rapidly deposited glacimarine sequences are constrained to a period of less than 450 kyr by our age model, suggesting that orbital influences at the frequencies of obliquity (40 kyr) and eccentricity (125 kyr) controlled the oscillations of the ice margin at that time. An erosional hiatus covering 250 kyr provides direct evidence for a major episode of global cooling and ice-sheet expansion about 23.7 Myr ago, which had previously been inferred from oxygen isotope data (Mi1 event[5]).

Sediment cores recovered from the Antarctic continental margin during the past three decades have indicated that grounded ice has covered much of Antarctica since Oligocene times[2–4,12], with the earliest ice sheets forming close to the Eocene/Oligocene boundary around 34 Myr ago[4–7]. Oligocene strata in the longest and most complete of these cores (CIROS-1) recorded cycles of ice-margin advance and retreat representing ice-volume changes that might have driven past sea-level fluctuations[3], such as those later inferred from high-resolution, deep-sea oxygen isotope records[5,9,10]. However, the frequency of these oscillations could not be determined. This was because core stratigraphy and sedimentology indicated numerous potential time breaks, and because core chronologies, based largely on biostratigraphic methods, allowed a time resolution of no better than a million years.

In the austral summers of 1998 and 1999, the Cape Roberts Project (CRP) drilled 1,500 m of strata from the western margin of the Victoria Land basin[13–15] (Fig. 1); 46 unconformity-bound, Oligocene to Early Miocene (33–17 Myr ago) glacimarine cycles, or depositional sequences, were recorded. The strata accumulated some kilometres off the coast as part of a laterally extensive seaward-thickening nearshore wedge. This geometry is evident in seismic profiles oriented parallel to and normal to the coast[16]. During periods of glacial advance, the interior ice sheet fed through outlet glaciers to a laterally extensive marine ice terminus that extended well out onto the continental shelf beyond the CRP drill sites. In periods of ice retreat the drill sites lay off an open wave-dominated coast, with deposition of mud, and occasional debris from floating ice. Thus cycles of ice-margin advance and retreat across the shelf are viewed as cycles of expansion and contraction of the East Antarctic ice sheet recorded as unconformity-bound sequences. This view is supported by the style of erosion within these strata—laterally extensive, sub-horizontal erosion surfaces, judging from coast-parallel seismic sections.

Each sequence (Fig. 2) begins with an erosion surface followed by a characteristic vertical facies succession, interpreted to represent: (1) erosion during ice-margin advance followed by deposition during ice-margin retreat, (2) relatively ice-free open marine sedimentation and (3) re-advance of the ice margin into a shallow marine setting. Sedimentary features of this succession are given in more detail below, but it is important to note that sedimentological and faunal palaeobathymetric indicators within cycles suggest that water depth changes of up to ~50 m occurred in concert with ice-margin advance and retreat cycles[13,14]. Variations in grain size and changes in lithofacies with time primarily reflect oscillations in depositional energy that were most probably controlled by the combination of changes in shoreline and glacial proximity. Such

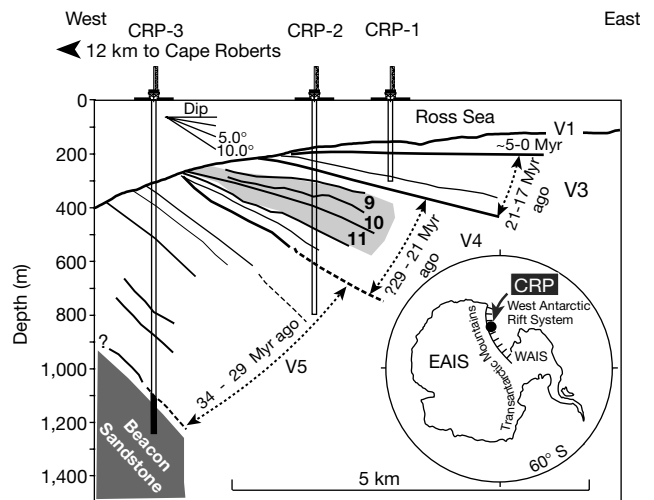Figure 1 Cross-section through Cenozoic strata beneath the western flank of Roberts ridge, western Ross Sea. The geometry and age of strata recovered by CRP drilling is shown. Depositional sequences 9, 10 and 11 in CRP-2/2A, the focus of this study, are mappable in seismic reflection profiles[16]. EAIS, East Antarctic ice sheet; WAIS, West Antarctic ice sheet. V1−5 refer to Ross Sea seismic units (see ref. 16).

719

inferences are consistent with established depositional models of temperate and polythermal (sub-polar) glaciers entering the sea[17], and with models of shallow marine sedimentation during orbitally driven cyclical changes in relative sea level[18].

Basal sequence boundaries are overlain by massive diamictite and sandstone. Clast fabrics are weakly oriented or random, suggesting a large component of rainout debris, which in many cases may have been remobilized in gravity flows. Subglacial shear is indicated by syndepositional soft sediment deformation structures, intraclasts, and clastic dykes within diamictites[19]. Subglacial features are indicated by 'turbate' and 'linear' microstructures and a pervasive 'plasmic' fabric, characterized by an oriented clay matrix, within diamictites and deformed sediments beneath diamictites[20]. The basal diamictite of sequence 11 (for example, Fig. 2) displays synsedimentary shearing and contains striated clasts[14]. Sequence boundaries are formed by erosional processes during ice advance and the overlying sediments, with their lack of ice-contact features and fining-upwards texture, are mostly the product of a retreating ice margin.

Basal sediments are followed by a sparsely fossiliferous, bioturbated shelf mudstone corresponding to an interval of maximum water depth, the glacial minimum, and the lowest sedimentation rate within a cycle. A sharp-based, shallow-marine, regressive sandstone facies succession occurs in the upper parts of most sequences. The shallowing character of this succession, and the truncation by the overlying sequence boundary, are both consistent with sediments deposited during a period of relative sea-level fall followed by erosion by the re-advancing ice margin.

Figure 2 shows systematic variations in grain size, clast content, diatom abundance and γ-radiation for one of the more fully developed depositional sequences in CRP-2/2A drill core (Fig. 1), sequence 11. These variations represent environmental proxies that provide additional support to the ice margin and relative water depth interpretations outlined above. The up-section decrease in sand content, clast abundance[21] (ice-rafted debris), and diatom abundance[22] in the lower part of sequence 11 is consistent with

progressive withdrawal of the ice margin from the Ross Sea in concert with a decrease in hydraulic energy during shoreline transgression and relative sea-level rise. The main peak in the number of *in situ* diatom tests corresponds to a mudstone interval within sequence 11, interpreted as ice-distal open shelf and indicative of increased oceanic connection during interglacials. In contrast, peaks in reworked diatom assemblages correspond to diamictites. The γ-ray log displays a positive shift from quartz- and plagioclase-rich, ice-proximal sandstone upward into an interval of high-potassium, illite-dominated, ice-distal shelf mudstone[23].

Most of the time interval spanned by the Cape Roberts drillcore is not represented by the stratigraphic record owing to non-deposition and erosion through long-term tectonic influences and shorter-term glacial processes[14,15]. However, intervals of relatively continuous deposition occur where increased rates of basin subsidence provided sufficient accommodation space. Thus, although fragmentary, the CRP record provides high-resolution windows into the history and dynamics of the East Antarctic ice sheet. One such interval includes sequences 9, 10 and 11 (Fig. 1) in the CRP-2/2A core. These sequences are on average much thicker than the rest, and include a number of high-precision age datums (polarity reversals and numeric ages on volcanic ashes) providing a chronology that allows estimation of sequence durations at Milankovitch periodicities (Fig. 3). This chronology, which is based on a combination of single-crystal $^{40}Ar/^{39}Ar$ ages[24], microfossil biostratigraphy[22,25], $^{87}Sr/^{86}Sr$ analyses[26], and correlation of a magnetic polarity zonation to the magnetic polarity timescale (MPTS)[27], permits the construction of a robust age model for sequences 9 to 11[28].

Single-crystal, laser-fusion $^{40}Ar/^{39}Ar$ tephra ages at 280 and 193 m below sea floor (m.b.s.f.), $^{87}Sr/^{86}Sr$ ages on *in situ* molluscan samples at 247 and 195 m.b.s.f., and the last occurrence (LO) of *Lisitzinia ornata* at 255 m.b.s.f. (in C6Cr in Southern Ocean cores[29]) constrain correlation of the normal-polarity interval (magnetozone N5) containing sequences 10 and 11 with geomagnetic chron C6Cn.3n. Stratigraphically higher magnetozones R4 and N4 comprising the lower three-quarters of sequence 9 are correlated with

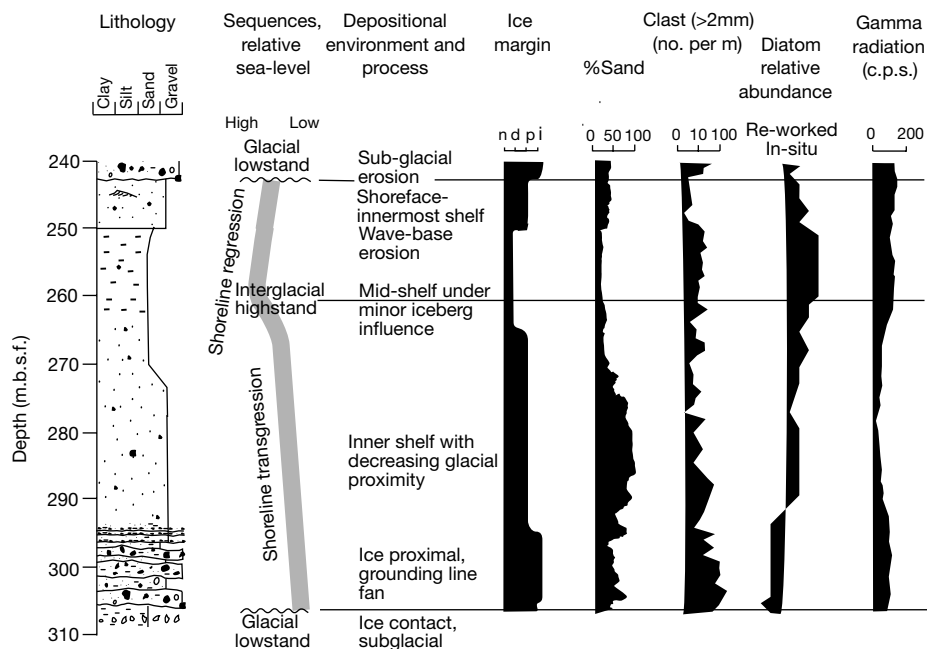**Figure 2** Lithological and environmental changes through sequence 11. Vertical variations in grain size, ice-rafted debris, diatom abundance and γ-radiation are shown for a more fully developed orbitally driven, ice advance–retreat–readvance cycle in CRP-2/2A. Key for the interpretation of ice margin proximity: n, non-glacial (marine); d, distal glacimarine; p, proximal glacimarine; i, ice contact[14].

C6Cn.2r and C6Cn.2n, respectively. The upper quarter of sequence 9, which has reversed polarity (magnetozone R3) and contains the LO of *Dictyococcites bisectus*, is correlated with earliest C6Cn.1r[30]. The age model implies an age range from 24.12 to 23.68 Myr. Given that the thin magnetically reversed interval (magnetozone R4) corresponds to rapidly deposited ice-proximal diamictite and sandstone at the base of sequence 9, most of the sedimentary record of C6Cn.2r is considered to have been lost at the underlying sequence boundary—perhaps as much as 250 kyr. The Oligocene/Miocene boundary is placed within sequence 9 at the base of C6Cn.2n at 183.70 m.b.s.f.[28].

An alternative age model has been proposed[28] that correlates sequence 9 (magnetozones R4, N4 and R3) with the upper part of C6Cn.3n. In this age model, the 4-m-thick reversed polarity interval of diamictite and sandstone at the base of sequence 9 is inferred to represent a short-duration geomagnetic excursion within C6Cn.3n, and the LO of *D. bisectus* in CRP-2/2A is correlated with C6Cn.2r in the earliest Miocene. This alternative age model has been considered unlikely[28] because: (1) the polarity signal is robust for the interval of CRP core, (2) the MPTS[31] contains no evidence of 'tiny wiggles' at

this time and sedimentary records from ODP site 1090 spanning C6Cn.3n show no indication of short polarity intervals (J. Channell, personal communication), and (3) the age of the LO of *D. bisectus* would be inconsistent with Southern Ocean records[30].

Our preferred age model restricts the duration of the three glacimarine sequences to no more than ~450 kyr. Sequence 9 is of ~125 kyr duration (C6Cn.2n spans 123 kyr), and may reflect orbital control of the East Antarctic ice sheet at the eccentricity frequency. The stratigraphically underlying sequences 10 and 11 are restricted to C6Cn.3n, a duration of 119 kyr. Moreover, with sequence 10 appearing to be truncated[13] and with most of C6Cn.2r inferred to be missing at the sequence 9/10 unconformity, we contend that sequences 10 and 11 probably reflect 40-kyr, obliquity-controlled oscillations in the margin of the East Antarctic ice sheet. On this basis, we present a correlation of sequences 9, 10 and 11 with a high-resolution, Late Oligocene–Early Miocene deep-sea oxygen isotope record from western Atlantic, ODP site 929[9,10] (Fig. 4).

Figure 4 shows a detailed characterization of the Mi1 oxygen isotope excursion[5], which is defined by an overall ~1.5‰ increase
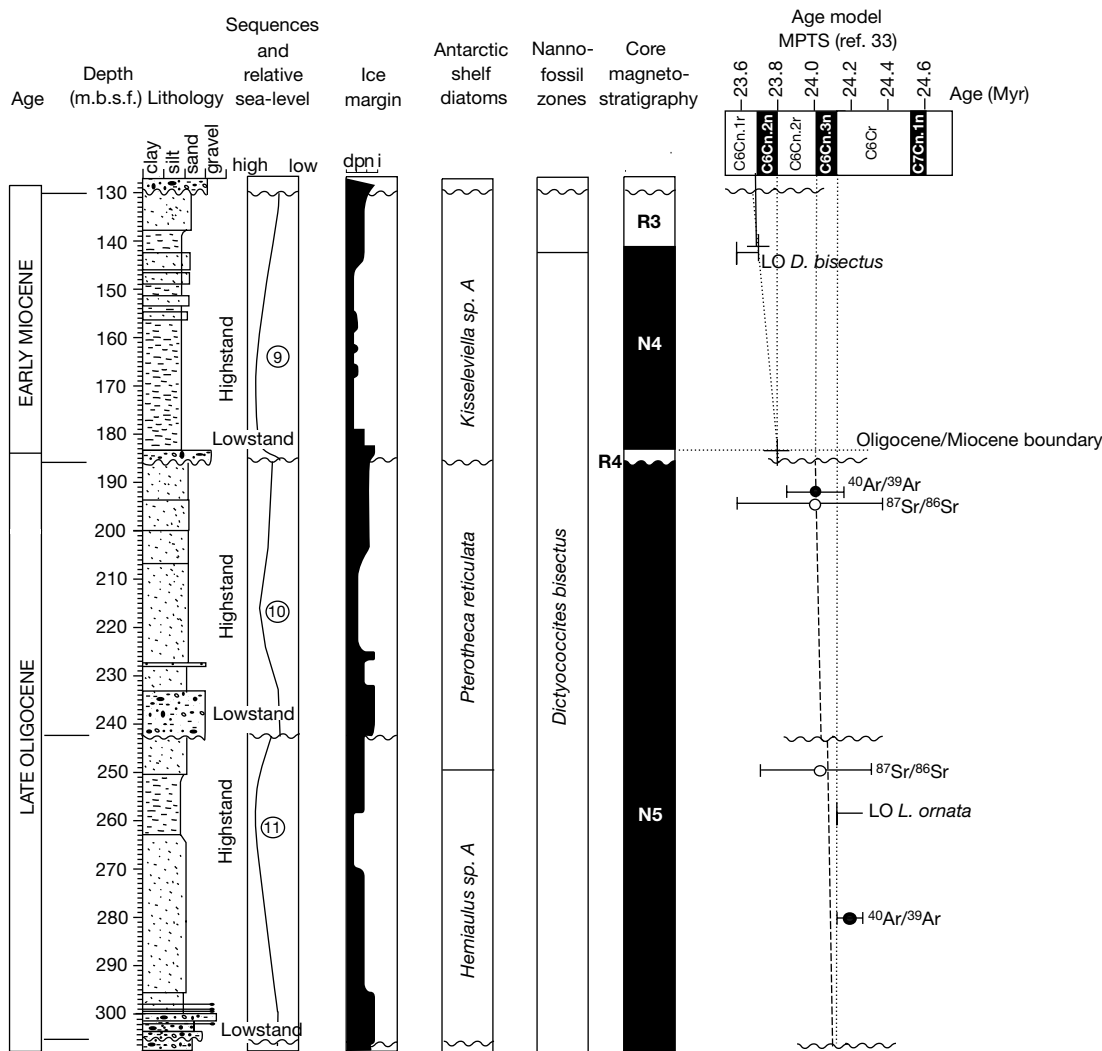
Figure 3 Lithostratigraphy, sequence stratigraphy, variation in sand content and age models for sequences 9, 10 and 11 (130.27–306.65 m) from the CRP-2/2A drill hole. Key for ice margin proximity is shown in Fig. 2 legend. Datums include: (1) the LO (last occurrence) of *Dictyococcites bisectus* at 144.44 m and LO of *Lisitzinia ornata* at 259.2 m in C6Cn.1r and C6Cr, respectively, (2) the $^{40}Ar/^{39}Ar$ pumice dates at 193.40 m

(23.98 ± 0.13 Myr) and at 280.03 m (24.22 ± 0.03 Myr) and (3) the $^{87}Sr/^{86}Sr$ dates on *in situ* mollusca at 194.87 m (24.00+0.4/-0.5 Myr) and 247.00 m (24.02 ± 0.35 Myr). The length of vertical bars on biostratigraphic datums indicates the range of error from the respective sampling interval on which the datums are defined.

in $\delta^{18}O$, equivalent to a sea-level lowering of $\sim$80 m accompanied by a decrease in deep-water temperature of 3 °C (refs 9, 10). The increase and subsequent decrease in oceanic mean $\delta^{18}O$ across the Mi1 event has been interpreted as a long-term, 400-kyr, eccentricity cycle[9]. Higher-frequency 100-kyr (eccentricity) and 40-kyr orbital (obliquity) components punctuate the Mi1 excursion. Strong covariance reported in the benthic and planktonic foraminiferal $\delta^{18}O$ record and the absence of a Northern Hemisphere ice sheet is taken to suggest the presence of retreating and advancing ice sheets on Antarctica[9]. Assuming a Pleistocene calibration of 0.11‰ $\delta^{18}O$ per 10 m of sea-level, sea-level fluctuations of $\sim$30–40 m are indicated at 40- and 100-kyr frequencies with corresponding changes in deep-water temperature of 1–2 °C. Like the authors of ref. 10, we find it intriguing that the climatic deterioration leading into the Mi1 event is punctuated by 40-kyr cycles, yet 100-kyr cycles dominate the $\delta^{18}O$ record after the Mi1 excursion. Although not well understood, certain periods of Earth history (for example, the past 800 kyr) have been dominated by a climatic response at 100-kyr orbital frequencies. This phenomenon has been explained by several mechanisms involving nonlinear responses to orbital forcing—these include feedbacks in ocean–atmosphere circulation, the global carbon cycle, and the internal dynamics and bedrock interactions associated with large continental ice sheets in polar regions[31].

In summary, the pattern of ice-volume change that is indicated by the deep ocean record (Fig. 4) is consistent with the pattern of ice marginal sedimentation on Antarctica implied from our analysis of the CRP-2/2A core for the interval 24.1–23.7 Myr ago. Oscillations in ice margin inferred from glacimarine sequences 11 and 10 can be correlated with 40-kyr, $\delta^{18}O$ cycles at the onset of the Mi1 excursion.

The erosional hiatus of some 250 kyr between sequences 10 and 9 spans an interval of major global cooling, ice-sheet expansion, and sea-level fall culminating at the Mi1 maximum. The oscillation in ice-margin proximity inferred from sequence 9 can be correlated with a $\sim$125-kyr, $\delta^{18}O$ cycle in the heavily eccentricity-modulated part of the record that follows the Mi1 excursion.

We conclude that the cyclicity recorded by glacimarine sequences in CRP-2/2A provides strong ice-marginal evidence for orbital oscillations in the size of the Oligocene East Antarctic ice sheet, a style of behaviour identical with that of the unstable Northern Hemisphere ice sheets of the past 2.5 Myr. Studies of Antarctic ice sheets during the Oligocene—a time when planetary temperature was around 3–4 °C warmer than today—should help to provide realistic analogues for their future behaviour following the increased levels of atmospheric CO_2 and temperature projected for the end of this century[32]. □

1. Freeman, K. H. & Hayes, J. M. Fractionation of carbon isotopes by phytoplankton and estimates of ancient CO_2 levels. *Glob. Biogeochem. Cycles* **6**, 185–198 (1992).
2. Barrett, P. J., Elston, D. P., Harwood, D. M., McKelvey, B. C. & Webb, P.-N. Mid-Cenozoic record of glaciation and sea-level change on the margin of the Victoria Land basin, Antarctica. *Geology* **15**, 634–637 (1987).
3. Barrett, P. J. (ed.) Antarctic Cenozoic history from CIROS-1 drillhole, McMurdo Sound. *DSIR Bull.* **245**, 1–254 (1989).
4. Hambrey, M. J., Ehrmann, W. U. & Larsen, B. Cenozoic glacial record of the Prydz Bay continental shelf, East Antarctica. *Proc. ODP Sci. Res.* **119**, 77–132 (1991).
5. Miller, K. G., Wright, J. D. & Fairbanks, R. G. Unlocking the ice house: Oligocene oxygen isotopes, eustasy and margin erosion. *J. Geophys. Res.* **96**, 6829–6848 (1991).
6. Wise, S. W., Breza, J. R., Harwood, D. M. & Wei, W. in *Controversies in Modern Geology* (eds Mueller, D., McKenzie, J. & Weissart, H.) 133–177 (Academic, San Diego, 1991).
7. Zachos, J. C., Breza, J. & Wise, S. W. Early Oligocene ice-sheet expansion on Antarctica: stable isotope and sedimentological evidence from Kerguelen Plateau, southern Indian Ocean. *Geology* **20**, 569–573 (1992).
8. Zachos, J. C., Quinn, T. M. & Salamy, K. A. High-resolution deep-sea foraminiferal stable isotope records of the Eocene-Oligocene climate transition. *Paleoceanography* **11**, 256–266 (1996).
9. Zachos, J. C., Flower, B. P. & Paul, H. Orbitally paced climate oscillations across the Oligocene/Miocene boundary. *Nature* **388**, 567–570 (1997).
10. Paul, H. A., Zachos, J. C., Flower, B. P. & Tripati, A. Orbitally induced climate and geochemical variability across the Oligocene/Miocene boundary. *Paleoceanography* **15**, 471–485 (2000).
11. Lear, C. H., Elderfield, H. & Wilson, P. A. Cenozoic deep-sea temperatures and global ice volumes from Mg/Ca in benthic foraminiferal calcite. *Science* **287**, 269–272 (2000).
12. Hays, D. E. *et al.* General synthesis. *Init. Rep. DSDP* **28**, 919–942 (1975).
13. Fielding, C. R., Naish, T. R., Woolfe, K. J. & Lavelle, M. A. Facies analysis and sequence stratigraphy of CRP-2/2A, Victoria Land Basin, Antarctica. *Terra Antartica* **7**, 323–338 (2000).
14. Cape Roberts Science Team. Studies from the Cape Roberts Project, Ross Sea, Antarctica, Initial report on CRP-2/2A. *Terra Antartica* **6**, 1–173 (1999).
15. Cape Roberts Science Team. Studies from the Cape Roberts Project, Ross Sea, Antarctica, Initial report on CRP-3. *Terra Antartica* **7**, 1–209 (2000).
16. Henrys, S. A. *et al.* Correlation of seismic reflectors with CRP2/2A, Victoria Land Basin, Antarctica. *Terra Antartica* **7**, 221–230 (2000).
17. Powell, R. D. A model for sedimentation by tidewater glaciers. *Ann. Glaciol.* **2**, 129–134 (1981).
18. Naish, T. R. & Kamp, P. J. J. Sequence stratigraphy of 6th order (41 k.y.) Pliocene-Pleistocene cyclothems, Wanganui Basin, New Zealand: A case for the regressive systems tract. *Geol. Soc. Am. Bull.* **109**, 978–999 (1997).
19. Passchier, S. Soft sediment deformation features in core from CRP-2/2A, Victoria Land Basin, Antarctica. *Terra Antartica* **7**, 401–412 (2000).
20. Van der Meer, J. J. M. Microscopic observations on the first 300 metres of CRP-2/2A, Victoria Land Basin, Antarctica. *Terra Antartica* **7**, 339–348 (2000).
21. Talarico, F., Sandroni, S., Fielding, C. F. & Atkins, C. Variability, petrography and provenance of basement clasts in core from CRP-2/2A. Victoria Land Basin, Antarctica. *Terra Antartica* **7**, 529–544 (2000).
22. Scherer R., Bohaty, S. & Harwood, D. Oligocene and lower Miocene siliceous microfossil biostratigraphy for CRP-2/2A, Victoria Land Basin, Antarctica. *Terra Antartica* **7**, 417–442 (2000).
23. Bücker, C., Wonik, T. & Jarrard, R. Analysis of downhole logging data from CRP-2/2A, Victoria Land Basin, Antarctica: a multivariate approach. *Terra Antartica* **7**, 299–310 (2000).
24. McIntosh, W. C. $^{40}Ar/^{39}Ar$ geochronology of tephra and volcanic clasts in CRP-2/2A, Victoria Land Basin, Antarctica. *Terra Antartica* **7**, 621–630 (2000).
25. Watkins, D. K. & Villa, G. Paleogene calcareous nannofossils from CRP-2/2A, Victoria Land Basin, Antarctica. *Terra Antartica* **7**, 443–452 (2000).
26. Lavelle, M. Strontium isotope stratigraphy and age model for CRP-2/2A, Victoria Land Basin, Antarctica. *Terra Antartica* **7**, 611–620 (2000).
27. Wilson, G. S., Florindo, F., Sagnotti, L., Roberts, A. & Verosub, K. Magnetostratigraphy of CRP-2/2A, Victoria Land Basin, Antarctica. *Terra Antartica* **7**, 631–646 (2000).
28. Wilson, G. S. *et al.* Chronostratigraphy of the CRP-2/2A, Victoria Land Basin, Antarctica. *Terra Antartica* **7**, 647–664 (2000).
29. Harwood, D. M. & Maruyama, T. Middle Eocene to Pleistocene diatom biostratigraphy of Southern Ocean sediments from the Kerguelen Plateau, Leg 120. *Proc. ODP Sci. Res.* **120**, 683–733 (1992).
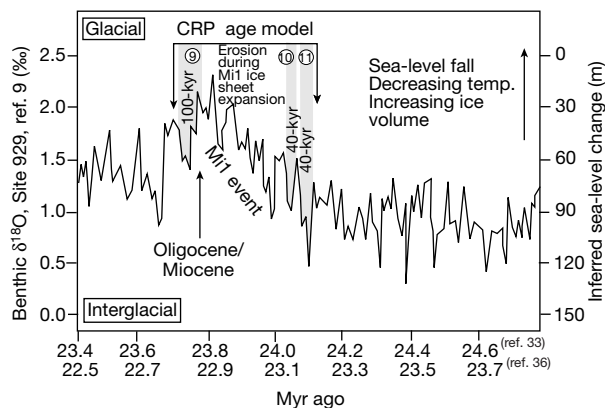

Figure 4 Correlation of sequences 9,10 and 11 in CRP-2/2A core, western Ross Sea with deep-water benthic foraminiferal $\delta^{18}O$ record of ODP site 929, western equatorial Atlantic. The $\delta^{18}O$ record has been interpreted as a proxy of Antarctic ice volume and oceanic temperature changes across the Oligocene/Miocene boundary[9,10]. Oscillations in the size of the East Antarctic ice sheet inferred from the ice-proximal CRP-2/2A core show a close correspondence with variations in the $\delta^{18}O$ record. Two age models have been proposed for the site 929 record. One is based on a nannofossil and planktonic foraminiferal biostratigraphy and, like our CRP-2/2A core data, is calibrated to the MPTS of ref. 33. Durations for intervals between biostratigraphic datums were estimated from inferred $\sim$40-kyr frequencies in magnetic susceptibility records. The second age model is based on a new astronomically calibrated timescale[34] established by tuning the 40-kyr cycles in magnetic susceptibility records to orbital target solutions for obliquity and precession[31]. The astronomical chronology has subsequently been used to recalibrate the MPTS in the vicinity of the Oligocene/Miocene boundary[36], and indicates that this boundary is $\sim$900 kyr younger than that reported in ref. 33. Because both age models for site 929 are based on a fundamental 40-kyr frequency in the magnetic susceptibility data, the durations of geomagnetic chrons and the frequency of the oxygen isotope signal is not affected by changes to absolute ages of the MPTS.

30. Hsü, K. J., Percival, S. F., Wright, R. & Peterson, N. P. Numerical ages of magnetostratigraphically calibrated biostratigraphic zones. *Init. Rep. DSDP* **73**, 625–635 (1983).

31. Imbrie, J. *et al.* On the structure and origin of major glaciation cycles 2. The 100,000 year cycle. *Paleoceanography* **8**, 699–735 (1993).

32. Houghton, J. *et al. Climate Change 2001: The Scientific Basis* (Third Assessment Report from IPCC Working Group 1), 1–944 (Cambridge Univ. Press, Cambridge, 2001).

33. Cande, S. C. & Kent, D. V. Revised calibration of the geomagnetic polarity time scale for the Late Cretaceous and Cenozoic. *J. Geophys. Res.* **100**, 6093–6095 (1995).

34. Shackleton, N. J., Crowhurst, S. J., Weedon, G. P. & Laskar, J. Astronomical calibration of Oligocene–Miocene time. *Phil. Trans. R. Soc. Lond. A* **357**, 1907–1929 (1999).

35. Laskar, J., Joutel, F. & Boudin, F. Orbital, precessional and insolation quantities for the Earth from −20Myr to +10Myr. *Astron. Astrophys.* **270**, 522–533 (1993).

36. Shackleton, N. J., Hall, M. A., Raffi, I., Tauxe, L. & Zachos, J. Astronomical calibration for the Oligocene–Miocene boundary. *Geology* **28**, 447–450 (2000).

. . . .

Agri-environment schemes do not effectively protect biodiversity in Dutch agricultural landscapes

David Kleijn, Frank Berendse, Ruben Smit & Niels Gilissen

Nature Conservation and Plant Ecology Group, Wageningen University, Bornsesteeg 69, 6708 PD Wageningen, The Netherlands

. . . .

Roughly 20% of the European Union's farmland is under some form of agri-environment scheme to counteract the negative impacts of modern agriculture on the environment[1]. The associated costs represent about 4% (1.7 billion euros) of the European Union's total expenditure on the Common Agricultural Policy and are expected to rise to 10% in the near future[2]. Although agri-environment schemes have been implemented in various countries for well over a decade, to date no reliable, sufficiently replicated studies have been performed to test whether such measures have the presumed positive effects on biodiversity[1,3,4]. Here we present the results of a study evaluating the contribution of agri-environment schemes to the protection of biodiversity in intensively used Dutch agricultural landscapes. We surveyed plants, birds, hover flies and bees on 78 paired fields that either had agri-environment schemes in the form of management agreements or were managed conventionally. Management agreements were not effective in protecting the species richness of the investigated species groups: no positive effects on plant and bird species diversity were found. The four most common wader species were observed even less frequently on fields with management agreements. By contrast, hover flies and bees showed modest increases in species richness on fields with management agreements. Our results indicate that there is a pressing need for a scientifically sound evaluation of agri-environment schemes.

Agri-environment schemes cover a wide range of measures, which differ depending on aim, country or even region, but have in common the basis that farmers are paid to adapt the management on (parts of) their farms to the benefit of biodiversity, environment

or landscape. Farmers participate on a voluntary basis, but once they enter a 'management agreement' they are obliged to adhere to a specified set of management prescriptions. We have investigated how effectively the most common form of agri-environment scheme—the management agreement[5]—conserves biodiversity on farms in The Netherlands.

The Netherlands has been implementing this type of agri-environment scheme since 1981, which is considerably longer than comparable European-Union-based measures (EEC regulation 2078/92) that have been introduced after 1992. Dutch agricultural landscapes are particularly important with respect to meadow birds in general, and the wader species black-tailed godwit (*Limosa limosa*) and oystercatcher (*Haematopus ostralegus*) in particular. Roughly 50% and 30–40%, respectively, of the European populations of these two species breed in The Netherlands[6]. As a consequence, most management agreements are aimed to support wader populations. Such agreements oblige farmers to postpone agricultural activities on individual fields until a set date, in June or July, allowing the birds to safely hatch their chicks.

A second type of management agreement is aimed at the conservation of species-rich vegetation in (edges of) grasslands and generally restricts the use of fertilizer and/or postpones the first mowing or grazing date. To evaluate their effectiveness, we used a pair-wise comparison of grassland fields that had long-running management agreements (on average 6 years) with nearby conventionally managed fields (for details see Supplementary Information).

Management agreements designed to enhance the botanical diversity of entire fields or field edges did not have any positive effect on vascular plant species richness in field edges (Fig. 1). No significant differences were found in the composition of the vegetation in edges of fields with or without management agreements. Furthermore, we did not find any correlation between age of the agreement and effect (the difference between each pair of control field and field with management agreement; data not shown). In 31,000 m^2 of field edge, we found 268, mostly very common, vascular plant species. A comparison between plant species composition of centre and edge (outer 2 m) of the fields showed that plant diversity in agriculturally used Dutch grasslands is a marginal matter indeed. On average, edges accounted for 96% of the total species richness of a field, and 66% of encountered species were never found in the field centre.

Interviews with farmers revealed that nitrogen inputs on fields with management agreements were lower than on conventionally managed fields (106 versus 246 kg N ha^{-1} yr^{-1}; *t*-test, $t_{34} = -2.62$, $P = 0.013$). Despite this considerable reduction in fertilizer inputs, the current level of inputs, in combination with nitrogen deposition rates of 35–55 kg N ha^{-1} yr^{-1} (ref. 7), may still be too high to promote the development of more species-rich vegetation or to enable less-competitive plant species to establish. In addition, seed
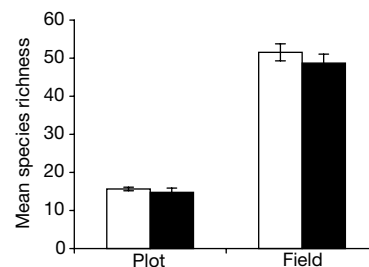

Figure 1 Effects of management agreements aimed at enhancing botanical diversity on number of plant species (mean ± s.e., $n = 22$) at plot (20 m^{-2}) and at field scale (400 m^{-2}; sum of 20 plots per field). Open columns, fields with management agreements; filled columns, conventionally managed fields.

723